Aspects of the Casimir effect in the sphere-plane geometry

Gert-Ludwig Ingold

Michael Hartmann, Paulo A. Maia Neto, Stefan Umrath

Universität Augsburg University

GEFÖRDERT VOM

Bundesministerium für Bildung und Forschung

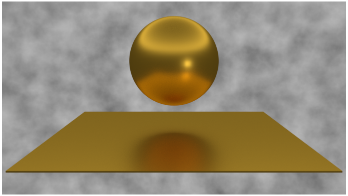

aspect ratio $\dfrac{R}{L}$ $R \leftarrow$ sphere radius, $L \leftarrow$ distance plane-sphere

$L \gg R$ origin of negative entropy – geometry and dissipation

Umrath, Hartmann, GLI, Maia Neto, Phys. Rev. E **92**, 042125 (2015)

$L \ll R$ numerics for large aspect ratios

corrections to PFA

Hartmann, GLI, Maia Neto, Phys. Rev. Lett. **119**, 043901 (2017)

Origin of negative entropy

Geometry and dissipation

Negative Casimir entropy

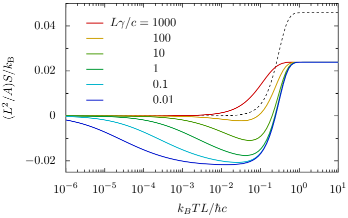

plane/plane, Drude metal

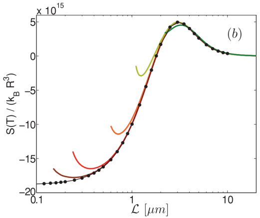

plane/sphere, perfect reflector

Canaguier-Durand, Maia-Neto, Lambrecht, Reynaud (2010)

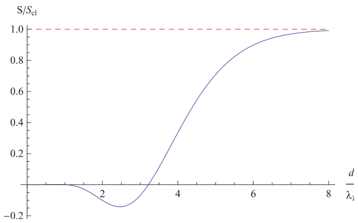

sphere/sphere, perfect reflector

Rodriguez-Lopez (2011)

A digression: Negative specific heat of the free damped particle

Specific heat for a system coupled to its environment

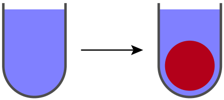

$$C = C_{S+B} - C_B$$

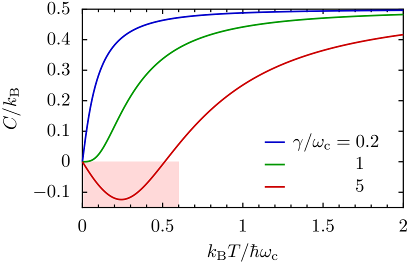

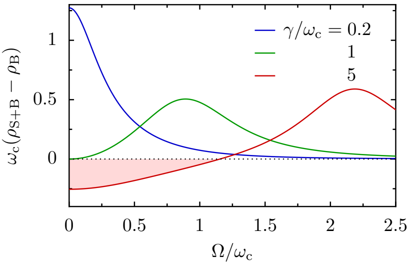

Hänggi, GLI, Talkner, New J. Phys. **10**, 115008 (2008)

GLI, Eur. Phys. J B **85**, 30 (2012)

level repulsion can lead to negative specific heat

Interaction entropy

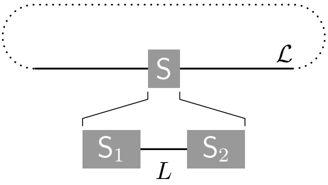

$$\frac{\det(\mathsf{S})}{\det(\mathsf{S}_1)\det(\mathsf{S}_2)} = \frac{1-\left[\bar{r}_1 r_2 \exp(2ikL)\right]^*}{1-\bar{r}_1 r_2 \exp(2ikL)}$$

for details see e.g.: GLI, Lambrecht, Am. J. Phys. **83**, 156 (2015)

Casimir energy

$$E_{\text{Cas}}(L) = \Delta E_{\text{vac}} - \Delta E_{\text{vac}}^{(1)} - \Delta E_{\text{vac}}^{(2)}$$

Casimir entropy

$$S_{\text{Cas}}(L) = \Delta S - \Delta S^{(1)} - \Delta S^{(2)}$$

Two sources of negative Casimir entropy

round-trip operator $\mathcal{M}(\xi) = \mathcal{R}_1(\xi)\mathcal{T}_{12}(\xi)\mathcal{R}_2(\xi)\mathcal{T}_{21}(\xi)$

free energy at high temperatures

$$\mathcal{F} = \frac{k_\mathrm{B} T}{2} \ln\left[\det\left(1 - \mathcal{M}(0)\right)\right]$$

entropy

$$\mathcal{S} = -\frac{\partial \mathcal{F}}{\partial T}$$

Two reasons why the roundtrip operator can vanish at zero frequency:

1. reflection operator $\mathcal{R}$
   electromagnetic response of scattering object
   ➢ Drude metal
2. translation operator $\mathcal{T}$
   polarization mixing ➢ geometry of scattering objects

Negative entropy induced by geometry

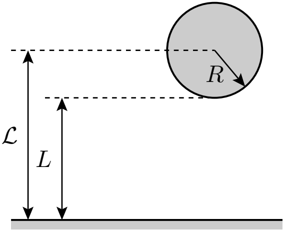

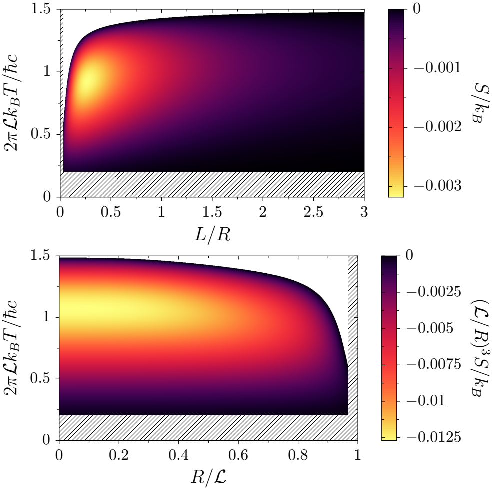

GLI, Umrath, Hartmann, Guérout, Lambrecht, Reynaud, Milton, Phys. Rev. E **91**, 033203 (2015)

→ **consider large distance limit**

Large-distance limit

- only one round-trip $\mathscr{R}_1\mathscr{T}_{12}\mathscr{R}_2\mathscr{T}_{21}$
- only dipole scattering ($\ell = 1$)
- small wave numbers dominate

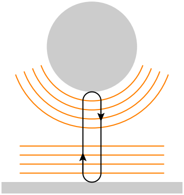

channel analysis

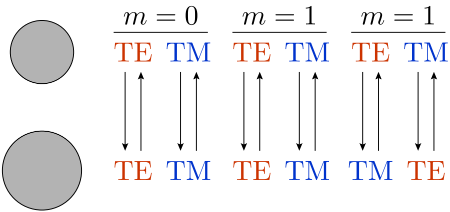

GLI, Umrath, Hartmann, Guérout, Lambrecht, Reynaud, Milton, Phys. Rev. E **91**, 033203 (2015)
Milton, Guérout, GLI, Lambrecht, Reynaud, J. Phys.: Condens. Matter **27**, 214003 (2015)

Reflection and translation

round-trip: $\mathscr{R}_1\mathscr{T}_{12}\mathscr{R}_2\mathscr{T}_{21}$

Mie coefficients

$$a_1^{\mathrm{PC}} = -\frac{2}{3}(kR)^3 + O(k^5) \qquad b_1^{\mathrm{PC}} = \frac{1}{3}(kR)^3 + O(k^5)$$

Translation coefficients

$$\mathscr{T}^{(0)}_{P,P} = 3\left(\frac{1}{(kd)^3} + \frac{1}{(kd)^2}\right)\exp(-kd)$$

$$\mathscr{T}^{(1)}_{P,P} = -\frac{3}{2}\left(\frac{1}{(kd)^3} + \frac{1}{(kd)^2} + \frac{1}{kd}\right)\exp(-kd)$$

$$\mathscr{T}^{(1)}_{P,P'} = \pm\frac{3}{2}\left(\frac{1}{(kd)^2} + \frac{1}{kd}\right)\exp(-kd) \qquad P \neq P'$$

- mode-mixing channels suppressed at small wave numbers
- free energy contribution vanishes at high temperatures
- negative contribution to the Casimir entropy

Negative entropy

The contribution of the polarization-mixing channel vanishes at high temperatures. → negative contribution to the entropy

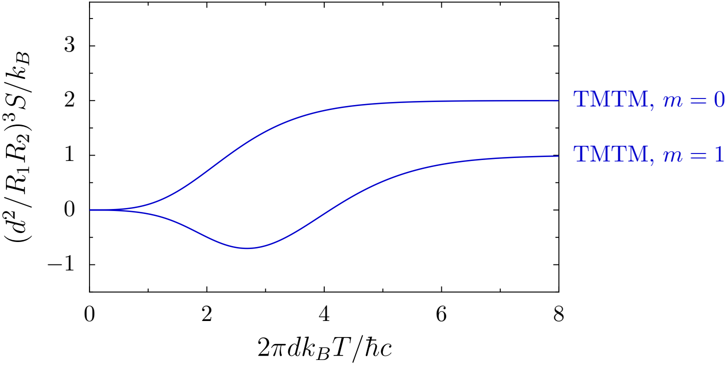

Negative entropy

The contribution of the polarization-mixing channel vanishes at high temperatures. → negative contribution to the entropy

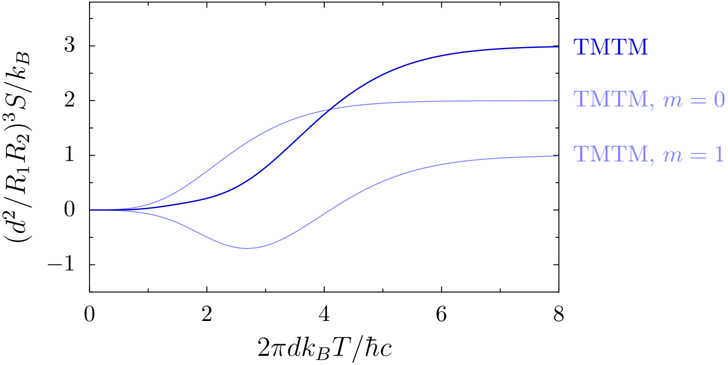

Negative entropy

The contribution of the polarization-mixing channel vanishes at high temperatures. → negative contribution to the entropy

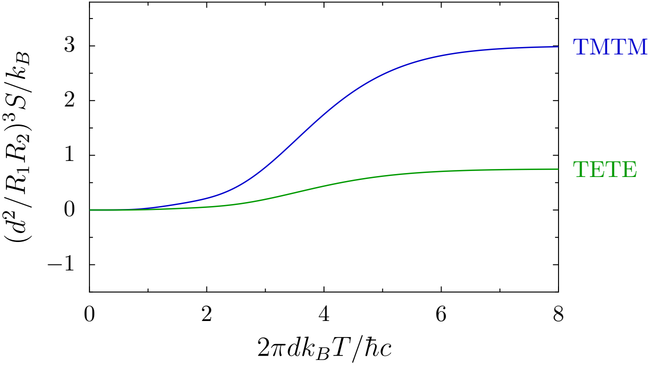

The contribution of the polarization-mixing channel vanishes at high temperatures. → negative contribution to the entropy

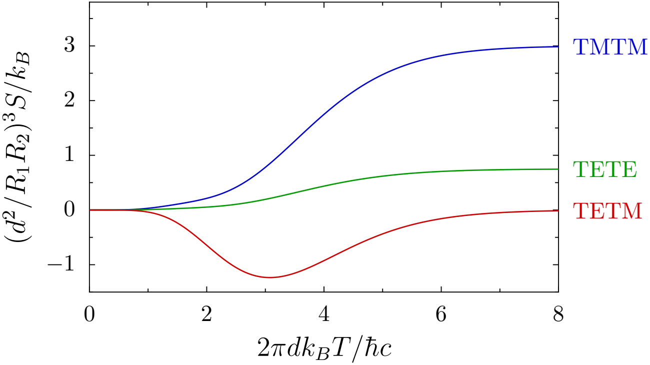

Negative entropy

The contribution of the polarization-mixing channel vanishes at high temperatures. → negative contribution to the entropy

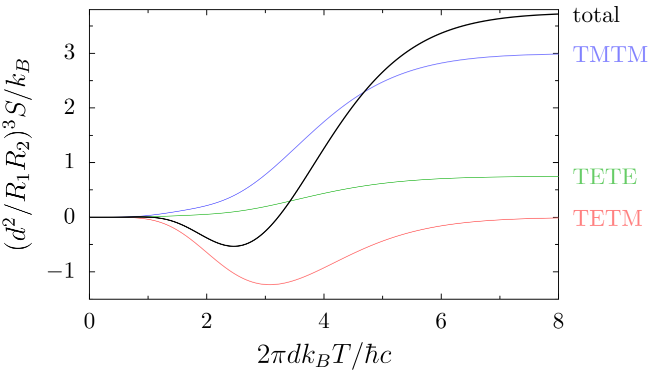

Free energy at weak damping

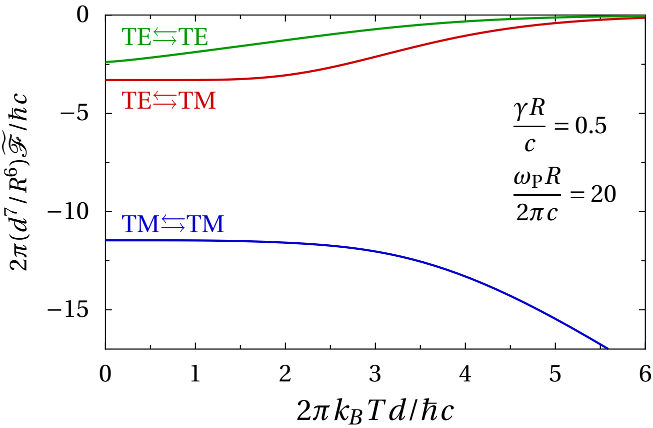

Umrath, Hartmann, GLI, Maia Neto, Phys. Rev. E **92**, 042125 (2015)

Channel analysis for weak damping

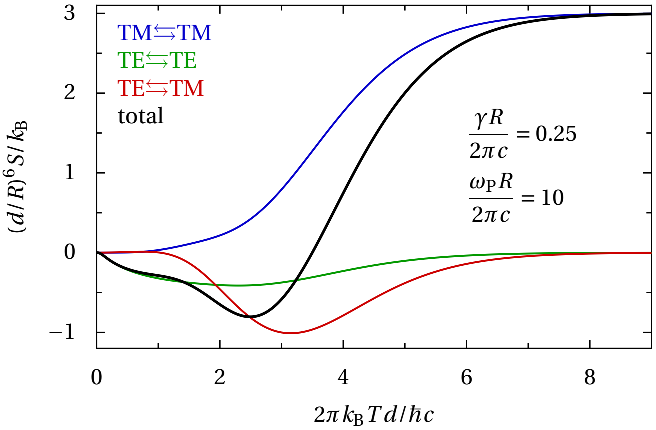

Umrath, Hartmann, GLI, Maia Neto, Phys. Rev. E **92**, 042125 (2015)

Channel analysis for weak damping

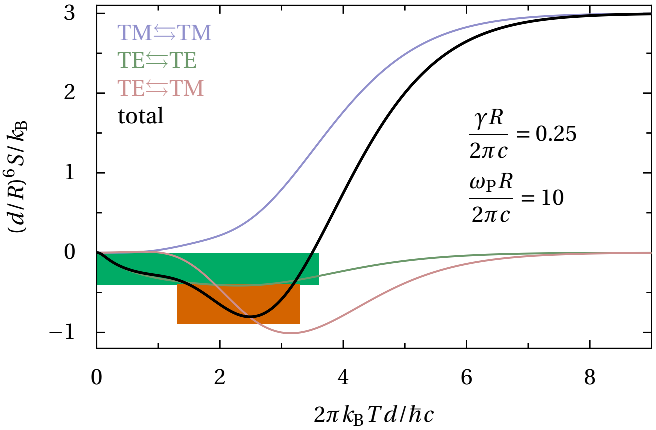

Umrath, Hartmann, GLI, Maia Neto, Phys. Rev. E **92**, 042125 (2015)

Numerics for large aspect ratios

Beyond PFA

Experimental aspect ratios

Universität Augsburg University

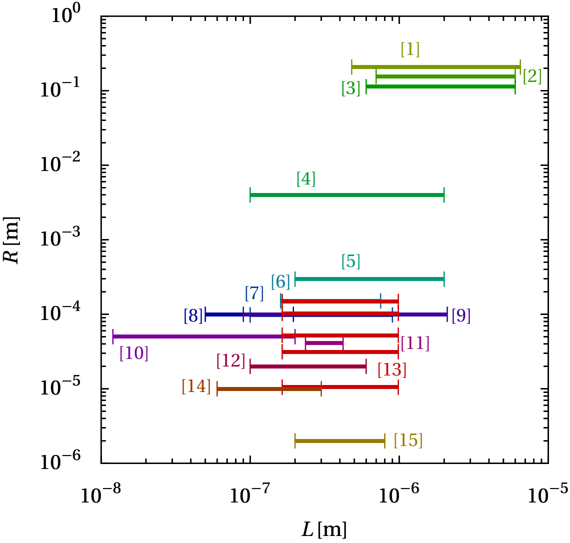

[1] Masuda, Sasaki (2009)
[2] Sushkov *et al.* (2011)
[3] Lamoreaux (1997)
[4] Garcia-Sanchez *et al.* (2012)
[5] Decca *et al.* (2003)
[6] Decca *et al.* (2007)
[7] Mohideen, Roy (1998)
[8] Man *et al.* (2009)
[9] Chan *et al.* (2001)
[10] van Zwol *et al.* (2008)
[11] Chang *et al.* (2012)
[12] Jourdan *et al.* (2009)
[13] Krause *et al.* (2007)
[14] Torricelli *et al.* (2011)
[15] Ether *et al.* (2015)

Experimental aspect ratios

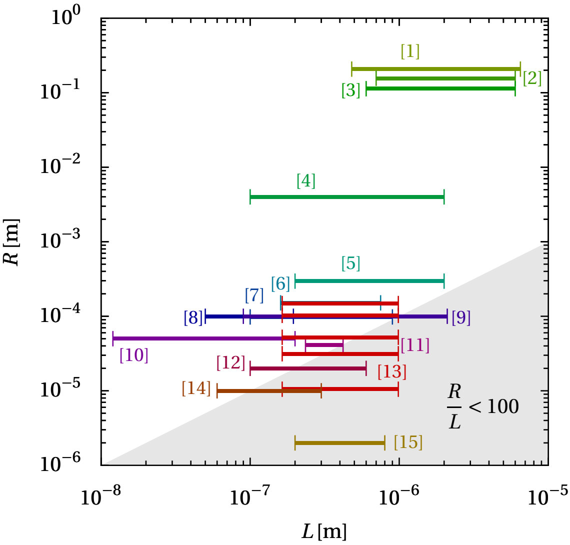

[1] Masuda, Sasaki (2009)
[2] Sushkov *et al.* (2011)
[3] Lamoreaux (1997)
[4] Garcia-Sanchez *et al.* (2012)
[5] Decca *et al.* (2003)
[6] Decca *et al.* (2007)
[7] Mohideen, Roy (1998)
[8] Man *et al.* (2009)
[9] Chan *et al.* (2001)
[10] van Zwol *et al.* (2008)
[11] Chang *et al.* (2012)
[12] Jourdan *et al.* (2009)
[13] Krause *et al.* (2007)
[14] Torricelli *et al.* (2011)
[15] Ether *et al.* (2015)

Experimental aspect ratios

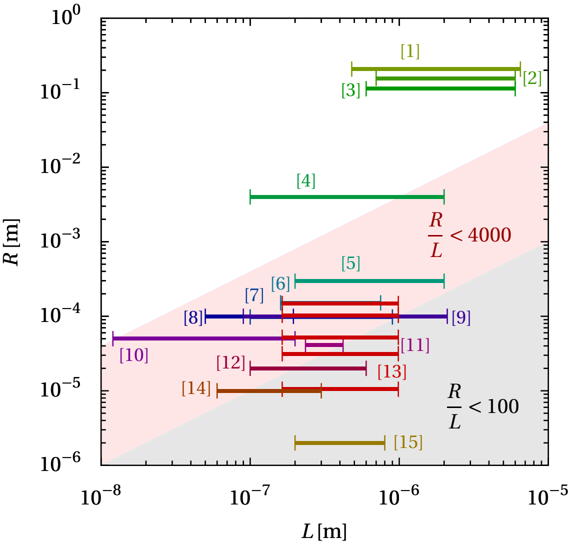

[1] Masuda, Sasaki (2009)
[2] Sushkov *et al.* (2011)
[3] Lamoreaux (1997)
[4] Garcia-Sanchez *et al.* (2012)
[5] Decca *et al.* (2003)
[6] Decca *et al.* (2007)
[7] Mohideen, Roy (1998)
[8] Man *et al.* (2009)
[9] Chan *et al.* (2001)
[10] van Zwol *et al.* (2008)
[11] Chang *et al.* (2012)
[12] Jourdan *et al.* (2009)
[13] Krause *et al.* (2007)
[14] Torricelli *et al.* (2011)
[15] Ether *et al.* (2015)

Round-trip operator

round-trip operator

$$\mathscr{M}(\xi) = \mathrm{e}^{-\mathscr{K}(L+R)}\mathscr{R}_\mathrm{P}\mathrm{e}^{-\mathscr{K}(L+R)}\mathscr{R}_\mathrm{S}$$

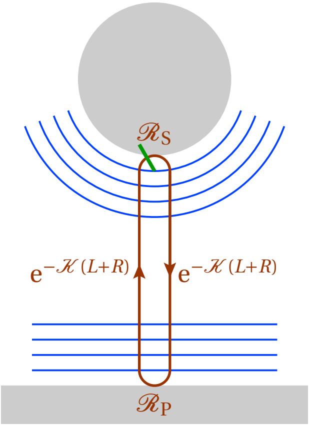

symmetrized round-trip operator

$$\widehat{\mathscr{M}}(\xi) = \sqrt{\mathscr{R}_\mathrm{S}}\mathrm{e}^{-\mathscr{K}(L+R)}\mathscr{R}_\mathrm{P}\mathrm{e}^{-\mathscr{K}(L+R)}\sqrt{\mathscr{R}_\mathrm{S}}$$

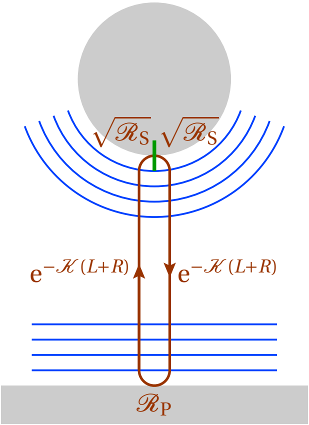

Matrix elements

Reduction of the dynamics of matrix elements by symmetrization

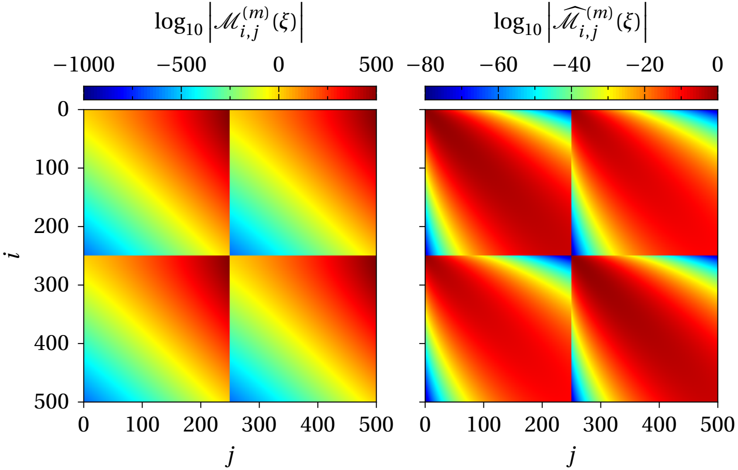

$\frac{L}{R} = 0.02 \quad m = 1 \quad \xi = \frac{c}{L+R}$

A closer look at the matrix elements

Universität
Augsburg
University

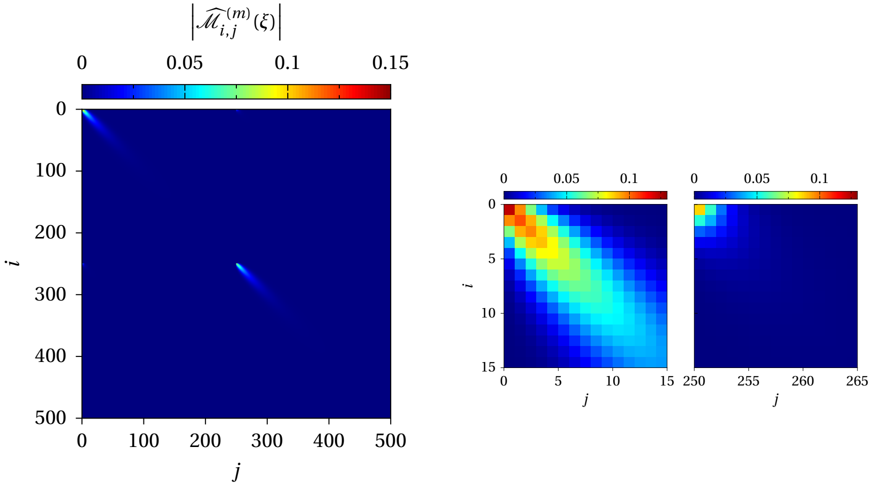

Performance improvement

Universität Augsburg University

hierarchical matrices

- subdivision into hierarchy of rectangular blocks
- approximation by low-rank matrices

→ data sparse matrices

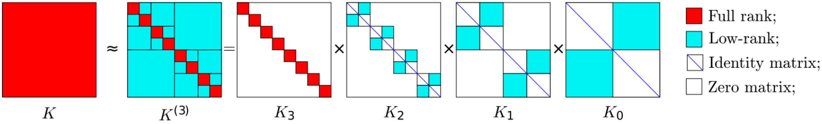

Ambikasaran, Darve, J. Sci. Comput. **57**, 477 (2013)

S. Ambikasaran, *A fast direct solver for dense linear systems* (2013)
https://github.com/sivaramambikasaran/HODLR

Performance improvement

Complexity of calculating a $N \times N$ determinant by LU decomposition: $\mathcal{O}(N^3)$

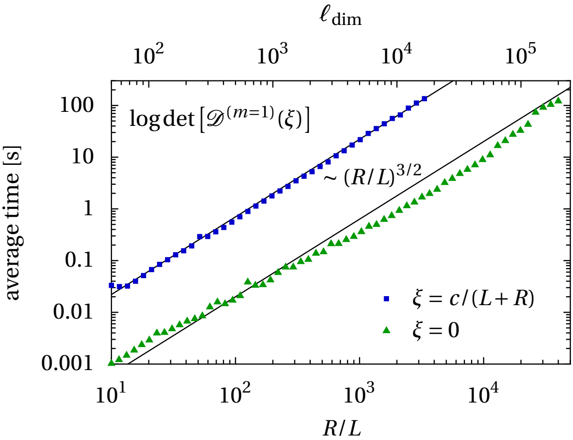

Optical properties of gold

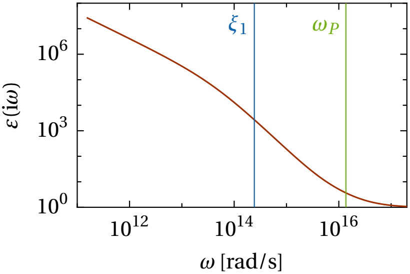

Palik, *Handbook of Optical Constants of Solids*
Lambrecht, Reynaud, Eur. Phys. J. D **8**, 309 (2000)

Zero-frequency contribution

- Drude model: TE mode not reflected
- plasma model: both modes are reflected

Difference described in terms of the high-temperature limit

the following data are for gold at room temperature

Corrections to the force beyond PFA

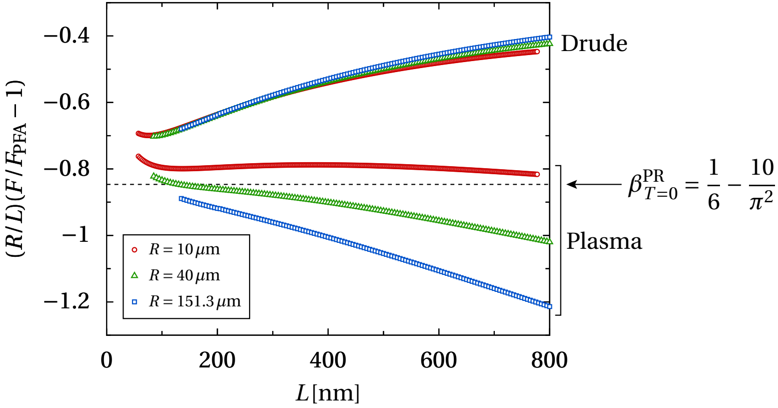

- for Drude model: correction independent of R for small L/R
- at larger distances, subleading order corrections become important
- for plasma model: structure of the derivative expansion result does not apply
- perfect reflector at $T = 0$ does not yield an upper bound on correction

Corrections to the force beyond PFA

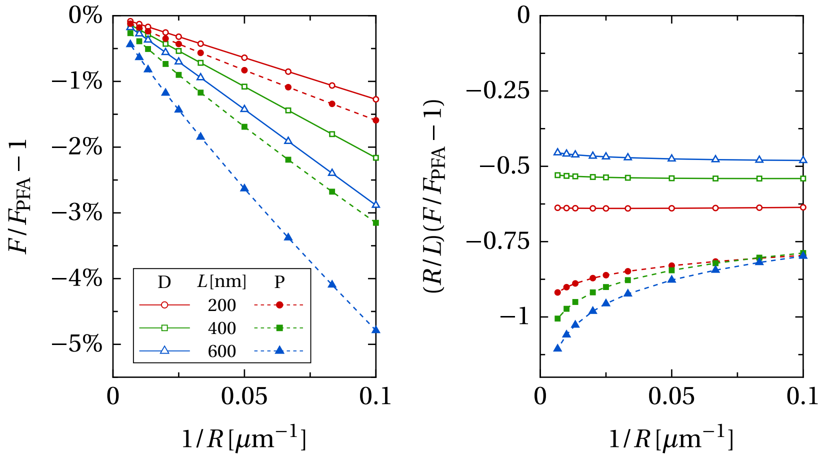

Limit on corrections beyond PFA

$$P^{\mathrm{eff}}(L,R) = -\frac{1}{2\pi R}\frac{\mathrm{d}F}{\mathrm{d}L} = P^{pp}(L)\left[1 + \beta'\frac{L}{R} + \dots\right]$$

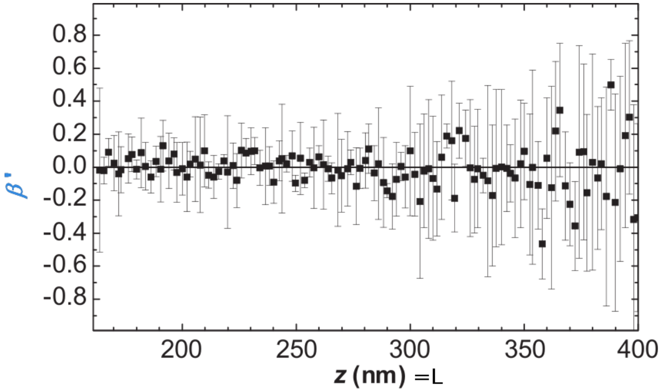

Krause, Decca, López, Fischbach, Phys. Rev. Lett. **98**, 050403 (2007)

PRL **98,** 050403 (2007) PHYSICAL REVIEW LETTERS week ending 2 FEBRUARY 2007

Experimental Investigation of the Casimir Force beyond the Proximity-Force Approximation

D. E. Krause,[1,2] R. S. Decca,[3] D. López,[4] and E. Fischbach[2]

[1]*Physics Department, Wabash College, Crawfordsville, Indiana 47933, USA*
[2]*Department of Physics, Purdue University, West Lafayette, Indiana 47907, USA*
[3]*Department of Physics, Indiana University-Purdue University Indianapolis, Indianapolis, Indiana 46202, USA*
[4]*Bell Laboratories, Lucent Technologies, Murray Hill, New Jersey 07974, USA*

(Received 21 June 2006; published 31 January 2007)

The analysis of all Casimir force experiments using a sphere-plate geometry requires the use of the proximity-force approximation (PFA) to relate the Casimir force between a sphere and a flat plate to the Casimir energy between two parallel plates. Because it has been difficult to assess the PFA's range of applicability theoretically, we have conducted an experimental search for corrections to the PFA by measuring the Casimir force and force gradient between a gold-coated plate and five gold-coated spheres with different radii using a microelectromechanical torsion oscillator. For separations $z < 300$ nm, we find that the magnitude of the fractional deviation from the PFA in the force gradient measurement is, at the 95% confidence level, less than $0.4z/R$, where R is the radius of the sphere.

Derivative expansion

- local expansion of the free energy
  - the upper hemisphere of the sphere may not contribute
- analyticity of the perturbative kernel
  - plasma model does not allow for derivative expansion

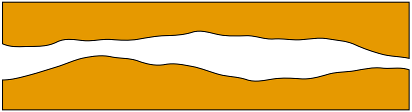

$$P^{\text{eff}}(L,R) = P^{pp}(L)\left[1 + \beta'(L)\frac{L}{R} + \dots\right]$$

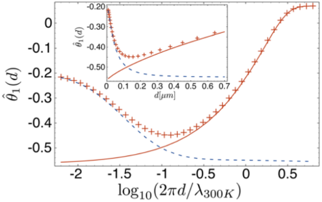

FIG. 2. (Color online) $\hat{\theta}_1$ for a gold sphere in front of a gold plate, computed using the tabulated optical data for gold, see Ref. 19. Crosses correspond to $T = 300$ K, while the dashed line is for $T = 0$ K. The solid line is for an ideal conductor at $T = 300$ K. For ideal conductors at $T = 0$, $\hat{\theta}_1 = -0.564$ independently of separation. The inset depicts the same data, for gold at 300 K, as a function of separation (in microns) on a linear scale.

- Fosco, Lombardo, Mazzitelli, PRD **84**, 105031 (2011)
- Bimonte, Emig, Kardar, EPL **97**, 50001 (2012)
- Bimonte, Emig, Kardar, APL **100**, 074110 (2012)
- Fosco, Lombardo, Mazzitelli, PRA **89**, 062120 (2014)
- Fosco, Lombardo, Mazzitelli, PRD **92**, 125007 (2015)

Bimonte, Emig, Kardar, APL **100**, 074110 (2012)

Corrections to the force gradient

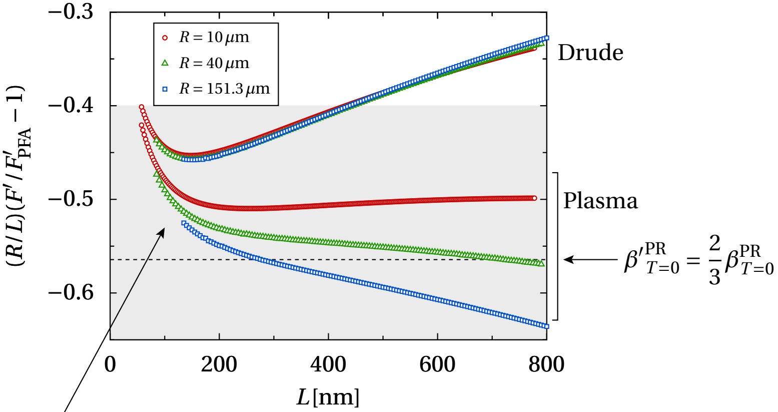

excluded by Krause, Decca, López, Fischbach, Phys. Rev. Lett. **98**, 050403 (2007)

- experimental bounds for β' violated for Drude and plasma model
- violation for plasma model more significant than for Drude model